# Combustion Synthesis of Triangular and Multifunctional $ZnO_{1-x}N_x$ ($x \leq 0.15$) Materials

Maitri Mapa and Chinnakonda S. Gopinath*

*Catalysis Division, National Chemical Laboratory, Dr. Homi Bhabha Road, Pune 411 008, India*

*Received November 10, 2008*

The preparation and characterization of multifunctional $ZnO_{1-x}N_x$ ($x \leq 0.15$) via a simple solution combustion method is reported. $ZnO_{1-x}N_x$ exhibits visible light absorption, thermal stability, nanometer-/micrometer-sized triangular particles, and catalytic properties. X-ray diffraction studies of $ZnO_{1-x}N_x$ demonstrate that the lattice oxygen in ZnO is replaced by nitrogen without any major change in the wurtzite structure; however, charge compensation occurs, because of interstitial Zn atoms, as well as oxygen vacancies. Microscopic studies reveal the dominance of nanometer- and micrometer-sized triangles of $ZnO_{1-x}N_x$. UV−visible and Raman spectra indicate a midgap state, derived from N 2*p* states, and direct Zn−N interaction, respectively. Secondary ion mass spectrometry studies show the presence of N and ZnN species in the bulk and support the direct Zn−N interaction. Electron paramagnetic resonance (EPR) studies indicate the presence of a small amount of defects. Photocatalytic decomposition of rhodamine B, and anisole acylation at room temperature, highlights the effectiveness of $ZnO_{1-x}N_x$ to catalysis applications. The aforementioned multifunctional characteristics suggest that $ZnO_{1-x}N_x$ might be used in place of conventional ZnO for better control and that it might be explored for further applications in catalysis and optoelectronics.

## Introduction

It is rare to find a material that exhibits many desired functional characteristics, ranging from magnetism to optical and catalysis. If a well-known system, such as ZnO, can be converted to one such system, it would attract attention both from the scientific and applications points of view. In fact, ZnO exhibits a unique property of a wide band gap (3.37 eV) with a free exciton binding energy (60 meV) at room temperature (RT), and it has many applications, from cosmetics to catalysis to optical lasers to space applications.[1,2] Doping in the ZnO lattice helps to reach many of the previously mentioned high-end applications.[3] Tuning the band gap by doping an heteroatom in the place of a Zn or O atom is a challenge. Among the heteroatoms, N is widely acceptable, because of its compatible size to O and the fact that it has the smallest ionization energy. To dope N into ZnO (N−ZnO), many sophisticated methods (such as molecular beam epitaxy, pulsed laser ablation, and chemical vapor deposition methods) have been utilized,[4] mainly toward optoelectronics applications, and yet there has been no breakthrough.[1] Indeed, poor nitrogen solubility in ZnO is an hindrance and, to date, nitrogen doping can be performed to a maximum of $10^{17}$ $cm^{-3}$,[1] or to a surface doping level of 6%.[5] Furthermore, the formation of Zn−O is energetically more favorable than the formation of Zn−N bonds. An enhancement of the doping level of nitrogen in ZnO and a reduction in the nitrogen acceptor levels are predicted to be required for the fabrication of low-resistive *p*-type ZnO.[5] Hence, a suitable method to prepare ZnO with a large nitrogen content could be helpful to enhance its utilization toward various applications, such as *p*-type conductors and photocatalysts, because of the delocalization effect.

ZnO is well-known to form oxygen vacancies, and a simple heating changes its color to pale yellow/brown at high temperatures, because of the oxygen vacancies, and it returns to being a colorless material at room temperature. We have used the aforementioned fact to introduce nitrogen into the ZnO lattice at high temperatures under combustion conditions, where a significant to large number of oxygen

* Author to whom correspondence should be addressed. Phone: 0091-20-25902043. Fax: 0091-20-2590 2633. E-mail: cs.gopinath@ncl.res.in. Website: www.ncl.org.in/csgopinath.

(1) (a) Klingshirn, C. *Chem. Phys. Chem.* **2007**, *8*, 782. (b) Özgur, Ü.; Alivov, Y. I.; Liu, C.; Teke, A.; Reshchikov, M. A.; Dogan, S.; Avrutin, V.; Cho, S. J.; Morkoc, H. *J. Appl. Phys.* **2005**, *98*, 041301. (c) Look, D. C.; Claftin, B.; Ya, I.; Park, S. J. *Phys. Status Solidi A* **2004**, *201*, 2203. (d) Nitienko, V. A. *J. Appl. Spectrosc.* **1992**, *52*, 367. (e) Pearton, S. J.; Norton, D. P.; Ip, K.; Heo, Y. W.; Steiner, T. *Prog. Mater. Sci.* **2005**, *50*, 293.

(2) (a) Karpina, V. A.; Lazorenko, V. I.; Lashkarev, C. V.; Dobrowolski, V. D.; Kopylova, L. I.; Baturin, V. A.; Pustovoytov, S. A.; Ju Karpenko, A.; Eremin, S. A.; Lytvyn, P. M.; Ovsyannikov, V. P.; Mazurenko, E. A. *Cryst. Res. Technol.* **2004**, *39*, 980. (b) Zhang, Z.; Lu, M.; Xu, H.; Chin, W.-S. *Chem. Eur. J.* **2007**, *13*, 632. (c) Velu, S.; Suzuki, K.; Gopinath, C. S. *J. Phys. Chem. B* **2002**, *106*, 12737. (d) Velu, S.; Suzuki, K.; Vijayaraj, M.; Barman, S.; Gopinath, C. S. *Appl. Catal. B: Environ.* **2005**, *55*, 287. (e) Maeda, K.; Domen, K. *J. Phys. Chem. C* **2007**, *111*, 7851.

(3) (a) Klingshirn, C.; Mollwo, E. *Z. Phys.* **1972**, *254*, 437. (b) Singh, A. V.; Mehra, R. M.; Wakahara, A.; Yoshida, A. *J. Appl. Phys.* **2003**, *93*, 396. (c) Orlinskii, S. V.; Schmidt, J.; Baranov, P. G.; Hoffmann, D. M. *Phys. Rev. Lett.* **2004**, *92*, 047603. (d) Maeda, K.; Teramura, K.; Takata, T.; Hara, M.; Saito, N.; Toda, K.; Inoue, Y.; Kobayashi, H.; Domen, K. *J. Phys. Chem. B* **2005**, *109*, 20504.

(4) (a) Volintiru, I.; Creatore, M.; van Helvoort, W. H.; Linden, J. L.; Van de Sanden, M. C. M. *Appl. Phys. Lett.* **2006**, *89*, 022110. (b) Bagnall, D. M. *Appl. Phys. Lett.* **1997**, *70*, 2230.

(5) (a) Perkins, C. L.; Lee, S. H.; Li, X.; Asher, S. E.; Coutts, T. J. *J. Appl. Phys.* **2005**, *97*, 034907. (b) Sanmyo, M.; Tomita, Y.; Kobayashi, K. *Chem. Mater.* **2003**, *15*, 819. (c) Yamamoto, T. *Thin Solid Films* **2002**, 420–421, 100.

10.1021/cm803048h CCC: $40.75 
Published on Web 12/19/2008

**Table 1. Physicochemical Characteristics of $ZnO_{1-x}N_x$ Materials**

| | lattice parameters (Å)[b] | | | | bulk (surface) content (at. %)[c] | | | | |
|---|---|---|---|---|---|---|---|---|---|
| $ZnO_{1-x}N_x$ code[a] | *a* | *c* | surface area ($m^2$/g) | density (g/$cm^3$)[f] | Zn | O | N | $(Zn/N)_{surf}$ | color |
| ZU1[d] | 3.2323 | 5.1784 | 1 | 5.81 | 24.4 | 60.5 | 15.1 | 72 | brownish orange |
| ZU1-650 | | | 1 | | 29.7 | 64.3 | 6.01 | | orange |
| ZU1-950 | 3.2511 | 5.2007 | 1 | 5.62 | 34.4 | 65.6 | | | off-white |
| ZU3 | 3.2390 | 5.1892 | 3 | 5.61 | 24.7 | 64.8 | 10.5 | 7.6 | orange |
| ZU5 | 3.2421 | 5.1924 | 7 | 5.58 | 19.7 | 70.7 | 8.6 | 6.3 | pale orange |
| ZU7 | 3.2414 | 5.1934 | 19 | 5.49 | 16.8 | 72.2 | 7.1 | 2.02 | pale orange |
| ZU10[e] | | | 102 | 5.23 | 14.9 | 55.1 | 0.2 | 0.58 | white |

[a] The urea:$Zn(NO_3)_2$ molar ratio is given after "ZU", followed by the calcination temperature (if any), in units of °C. [b] Lattice parameters for pure ZnO ($a$ = 3.25 Å and $c$ = 5.205 Å).[8] [c] Bulk and surface atomic content, measured from energy-dispersive X-ray analysis (EDX) and X-ray photoelectron spectroscopy (XPS), respectively. [d] ZU0.8 (with a urea:$Zn(NO_3)_2$ ratio of 0.8) exhibits characteristics similar to those of ZU1. [e] The bulk carbon content of ZU10 is 29.8 at. % and surface Zn:C atomic ratio from carbonate is 0.98. The carbon content is 1 and 3.9 at. % on ZU5 and ZU7, respectively. [f] Density of ZnO is 5.606 g/$cm^3$.[1]

vacancies should be available. In our recent efforts to make N−ZnO through the solution combustion method (SCM),[6] we have discovered a new ZnO material with the wurtzite structure and large bulk nitrogen content (15 at. %); because of the large nitrogen content, it may be called $ZnO_{1-x}N_x$. Structural, spectroscopy, mass spectrometry, microscopy, magnetic measurements were made, and applications in catalysis have been explored. $ZnO_{1-x}N_x$ exhibits a variety of properties, such as visible light absorption, triangular/prism-shaped and nanometer-/micrometer-sized crystals, high thermal stability, and catalytic activity. It is rare to find widely varying functional characteristics in one material, and it might be beneficial to explore $ZnO_{1-x}N_x$ for new and existing applications of ZnO, as different functionalities could be coupled for a better performance and/or process control.

## Experimental Section

**Synthesis.** All the chemicals were of analytical grade and used as such, without further purification. $Zn(NO_3)_2 \cdot 6H_2O$ (Merck) was used as a zinc precursor, and urea (Merck) was used as fuel. Starting chemicals from other manufacturers were also used. For the synthesis of ZU1 (the numeral given in the sample codes immediately after ZU indicates the mole ratio of urea/$Zn(NO_3)_2$ used) (see Table 1), equimolar amounts (0.04 mol) of $Zn(NO_3)_2 \cdot 6H_2O$ and urea were placed in a 250-mL beaker with 5 mL of distilled water. The aforementioned mixture was stirred until a uniform solution resulted, and then the mixture was inserted into a muffle furnace that was maintained at 500 °C. Water evaporates within the first few minutes, followed by ignition of the reactant mixture, with yellow flames, yielding a solid $ZnO_{1-x}N_x$ material. The solid product was collected after the completion of the combustion process. Other $ZnO_{1-x}N_x$ compositions also have been prepared using the same method, but with different urea/$Zn(NO_3)_2$ molar ratios of 0.8, 1, 3, 5, 7, and 10 (see Table 1).

**Characterization Methods.** Powder X-ray diffraction (XRD) data of $ZnO_{1-x}N_x$ materials was collected on a Rigaku X-ray diffractometer (Model DMAX IIIVC) that was equipped with a graphite crystal monochromator and used nickel-filtered Cu Kα radiation ($\lambda$ = 1.542 Å). Selected XRD data from the samples were collected on Philips X'Pert Pro diffractometer. The data were collected with a step size of 0.02° and a scan rate of 0.5°/min. The sample was rotated throughout the scan for better counting statistics. The observed interplanar *d*-spacing was corrected, with respect to silicon. Rietveld refinement of the selected powder XRD profiles was performed using the X'Pert Plus software. The surface area of the samples was estimated by $N_2$-adsorption/desorption isotherms, measured at −196 °C (QuantaChrome, Model NOVA 1200 equipment). Scanning electron microscopy (SEM) and energy-dispersive X-ray (EDX) measurements were performed on an SEM system (Leica, Model Stereoscan-440) equipped with a Phoenix EDX attachment. EDX spectra were recorded in the spot-profile mode by focusing the electron beam onto specific regions of the sample. Calibration of the experiment for nitrogen estimation was measured with several mixtures of gallium nitride and alumina powder. Thermal analysis experiments were peformed using thermogravimetry and differential thermal analysis (TG/DTA) (Perkin−Elmer, Diamond) at a rate of 10 °C/min in an air atmosphere for all materials. $Al_2O_3$ was used as an internal standard. Secondary ion mass spectroscopy (SIMS) studies were performed with a QMS-based instrument (Hiden Analytical). Bombardment was done with 5 keV O and Cs ions. The primary ion current was 400 nA for the oxygen beam and 100 nA for the cesium beam. The beam was rastered over an area of 1000 $\mu m^2$; however, the secondary ions were collected from the central area of 200 $\mu m^2$.

Diffuse reflectance UV−vis measurements were performed on a spectrophotometer (Shimadzu, Model UV-2550) with spectral-grade $BaSO_4$ as the reference material. Raman spectra were recorded on a Raman microscope (Ranishaw Model 2000) that was excited with a 633-nm laser. X-ray photoelectron spectroscopy (XPS) spectra were recorded on a VG Microtech Multilab ESCA 3000 spectrometer that was equipped with an Al Kα X-ray source ($h\nu$ = 1486.6 eV).[7] Binding energy (BE) calibration was performed with Au ($4f_{7/2}$) core level at 83.9 eV. Magnetization measurements were performed using vibrating sample magnetization in a physical property measuring system (PPMS; Quantum Design, USA).

Photocatalysis measurements were performed with a double-jacketed quartz reactor that was equipped with a 400-W mercury lamp, through the decomposition of rhodamine B. Water circulation in the outer jacket of the above reactor maintains the solution temperature at 25 °C. The absorption spectrum of the rhodamine B solution was obtained from an ultraviolet-visible-light (UV−vis) spectrometer (Shimadzu, Model UV-2500PC). Anisole acylation experiments were also performed with $ZnO_{1-x}N_x$ materials. Anisole acylation products were analyzed via gas chromatography (GC) equipment (Agilent, Model 6890 J-413) that consisted of a HP-5.5% phenyl methyl siloxane capillary column that was equipped for flame ionization detection (FID) and gas chromatography−mass

(6) (a) Murugan, B.; Ramaswamy, A. V.; Srinivas, D.; Gopinath, C. S.; Ramaswamy, V. *Chem. Mater.* **2005**, *17*, 3983. (b) Murugan, B.; Ramaswamy, A. V.; Srinivas, D.; Gopinath, C. S.; Ramaswamy, V. *Acta Mater.* **2008**, *56*, 1461. (c) Bera, P.; Aruna, S. T.; Patil, K. C.; Hegde, M. S. *J. Catal.* **1999**, *186*, 36. (d) Bera, P.; Priolkar, K. R.; Gayen, A.; Sarode, P. R.; Hegde, M. S.; Emura, S. *Chem. Mater.* **2003**, *15*, 2049.

(7) (a) Mathew, T.; Rao, B. S.; Gopinath, C. S. *J. Catal.* **2004**, *222*, 107. (b) Mathew, T.; Shiju, N. R.; Sreekumar, K.; Rao, B. S.; Gopinath, C. S. *J. Catal.* **2002**, *210*, 405.

(8) Kisi, E. H.; Elcombe, M. *Acta. Crystallogr., Sect. C* **1989**, *45*, 1865.

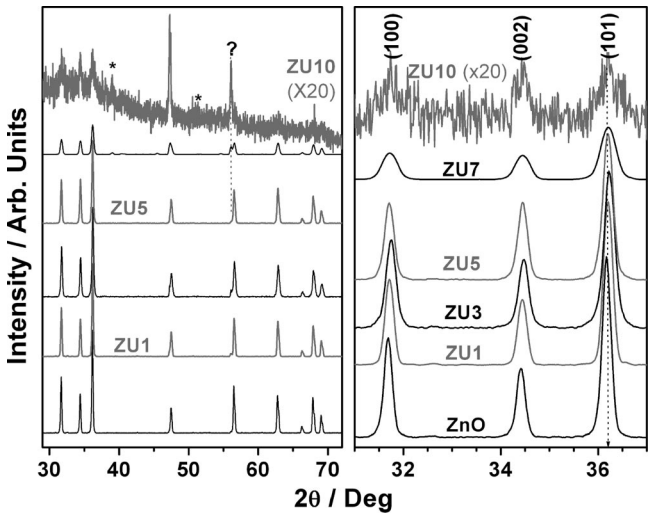


**Figure 1.** Powder X-ray diffraction (XRD) patterns of $ZnO_{1-x}N_x$ materials and ZnO. The expanded region between 31° and 37°, to show the peak shift and broadening, is shown in the right panel. The peak marked with an asterisk (∗) is due to $ZnCO_3$ on the ZU7 and ZU10 samples.[9] The peak with a question mark (?) at 56° is yet to be identified.

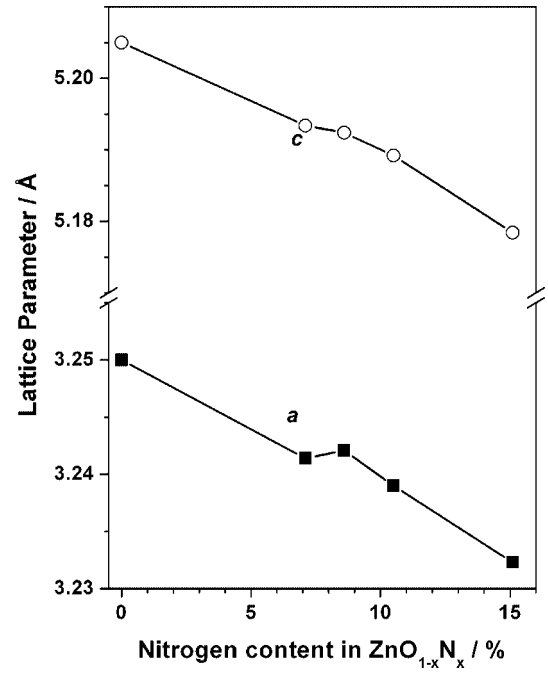


**Figure 2.** Lattice parameters of $ZnO_{1-x}N_x$ materials calculated from Rietveld analysis of the powder XRD data.

spectroscopy (GC-MS) (Shimadzu, Model GC-17A, coupled with a Model QP 5000 mass spectrometer).

## Results and Discussion

$ZnO_{1-x}N_x$ materials were prepared using different ratios of zinc nitrate to urea, via SCM, and a list of $ZnO_{1-x}N_x$ materials that were prepared is given in Table 1 with the physicochemical properties. The ratio of urea to zinc nitrate was varied between 0.8 and 10. The amino group in urea molecule is expected to be the main source for nitrogen introduction into the ZnO lattice under the aforementioned combustion conditions, because the simple calcination of $Zn(NO_3)_2 \cdot 6H_2O$ leads exclusively to ZnO. Assuming all the oxygen vacancies are filled with N atoms, the following reaction would be likely for equimolar amount of reactants:

$$Zn(NO_3)_2 \cdot 6H_2O + NH_2CONH_2 + (1 - 0.5x)O_2 \rightarrow ZnO_{1-x}N_x + (1 - 0.5x)N_2 + CO_2 + 8H_2O + 2NO_2$$

As the urea content increases, it produces more $CO_2$, and the exothermicity of the reaction increases linearly, because of better combustion. This is clearly reflected in the crystallinity, particle morphology and large bulk-nitrogen content in $ZnO_{1-x}N_x$ that is observed with lower urea amounts; however, the aforementioned situation changes diagonally to no clear particle morphology, poor crystallinity and preferential surface nitrogen doping with high urea content.

Figure 1 shows the XRD patterns of $ZnO_{1-x}N_x$ materials, along with that of ZnO. All diffraction features from $ZnO_{1-x}N_x$ materials could be indexed to the ZnO lattice,[8] and no additional peaks have been observed due to nitrogen introduction into the ZnO lattice. The aforementioned observation clearly demonstrates the formation of the hexagonal wurtzite structure. There is a small shift to higher diffraction angles associated with $ZnO_{1-x}N_x$ materials, compared to ZnO, indicating an overall contraction of the lattice. Significant amount of zinc carbonate formation[9] is evident from the XRD patterns of ZU7 and ZU10, because of the high urea content in the reaction mixture. Indeed, there is a small change in the lattice parameters and it is dependent on the amount of urea used in the preparation. Rietveld analysis of the XRD patterns (Figure 2) clearly suggests that the largest decrease in the lattice parameters (*a* and *c*) is observed with ZU1, which also shows the maximum nitrogen content (15.1 at. %), compared to ZnO. The lattice contraction observed with $ZnO_{1-x}N_x$ decreases as the urea content in the preparation increases and the lattice parameter moves closer toward ZnO.

EDX analysis demonstrates a low Zn:N ratio for ZU1, with a brown color and 15.1 at. % nitrogen, directly supporting the largest oxygen replacement by nitrogen. ZU3 shows a decrease in the N atom content to 10.5% and a simultaneous increase in O atom content to 64.8%. This directly suggests that the introduction of nitrogen is at the expense of oxygen. In contrast, the lowest nitrogen content observed on ZU10 is due to preferential surface nitrogen doping with large carbonate formation, and this will be discussed later. The N atom content in $ZnO_{1-x}N_x$ decreases as the urea content used in the initial reactants mixture increased. However, the O atom content increases with the urea content between ZU1 and ZU5. The aforementioned observations support the belief that the N atoms occupy the O lattice positions in ZnO. However, a small amount of nitrogen in the extra lattice positions cannot be excluded, although it is not detected in any of the characterization methods used in the present study. Peak broadening and low intensity observed in the XRD analysis for ZU7 and ZU10 with a simultaneous increase in the surface area, and a change in sample color toward white

(9) Effenberger, H.; Mereiter, K.; Zemann, J. *Z. Kristallogr.* **1981**, *156*, 233.

should be noted (see Table 1). Diffraction peaks due to zinc carbonate[9] was also observed in the XRD analysis and are indicated by an asterisk symbol (∗) in Figure 1. EDX and XPS analyses demonstrate the presence of carbon as a carbonate (or carbonate-like) species (see Figure SI-1 in the Supporting Information). Urea is a good fuel,[6] and combustion produces more $CO_2$ with more urea: this is the reason for increased carbonate formation on ZU7 and ZU10. Effective combustion might be a reason for the surface segregation (or surface doping) of nitrogen on ZnO in ZU7 and ZU10. Indeed, carbonate formation with more urea changes the atom percentage trend observed for materials with urea:$Zn(NO_3)_2$ > 5 (above ZU5). Also note that the atom content measured via EDX on individual particles differs significantly, and the values reported in Table 1 are the average values obtained over a large area. Our efforts to measure the nitrogen content using the Kjeldhal method with $ZnO_{1-x}N_x$ materials did not give meaningful results, unlike that observed with organic compounds and peptides. This is also a reason for the measurement of nitrogen content in $ZnO_{1-x}N_x$ materials via analytical methods.

Note that a significant difference in the density values of $ZnO_{1-x}N_x$ materials were observed, compared to that of ZnO (5.606 g/cm$^3$) (see Table 1). ZU1 (and ZU0.8) especially exhibits higher density (5.81 g/cm$^3$) than all other compositions and ZnO, suggesting a considerable change in composition and/or compact nature of the material. A large amount of nitrogen and a higher density indicates that some amount of interstitial Zn might be present in the lattice. Indeed, interstitial Zn and oxygen vacancies (vide supra, EPR studies) present in the lattice are mainly present to compensate for the excess anionic charge from the significantly large nitrogen content (15%) and to maintain the charge neutrality of the entire lattice. This is further supported by a decrease in the lattice parameter with increasing nitrogen content. In view of this, the actual stoichiometry of ZU1 would be $Zn_{1+\delta}O_{0.85}N_{0.15}$, and the value of $\delta$ is expected to be up to 0.05, from density values. Furthermore, the low surface area value that is observed for ZU1 (1 m$^2$/g) and the higher density corroborates well and supports the compact nature of ZU1. When ZU1 is subjected to air calcination at 950 °C, the material turns colorless and the density value of ZU1-950 (5.62 g/cm$^3$) is similar to that of ZnO (see Table 1), which supports the removal of nitrogen from the ZU1 lattice and a simple oxidation to ZnO. The low surface area observed after the aforementioned calcination with ZU1-950 is due to the sintering effect. Density values observed for ZU3 and ZU5 is comparable to that of ZnO; furthermore, the surface area also increases significantly and corresponds to a decreasing nitrogen content, indicating a decreasing interstitial Zn content in ZU3 and ZU5. A large increase in the surface area and a significant decrease in the density values of ZU7 and ZU10 suggests an increasing porosity of these materials. Furthermore, the nitrogen content decreases along with a change in the nature of materials that contain more carbonates (see Figure 1 and Table 1), clearly indicating that the effective introduction of nitrogen can be performed with a stoichiometric amount of urea and zinc nitrate.

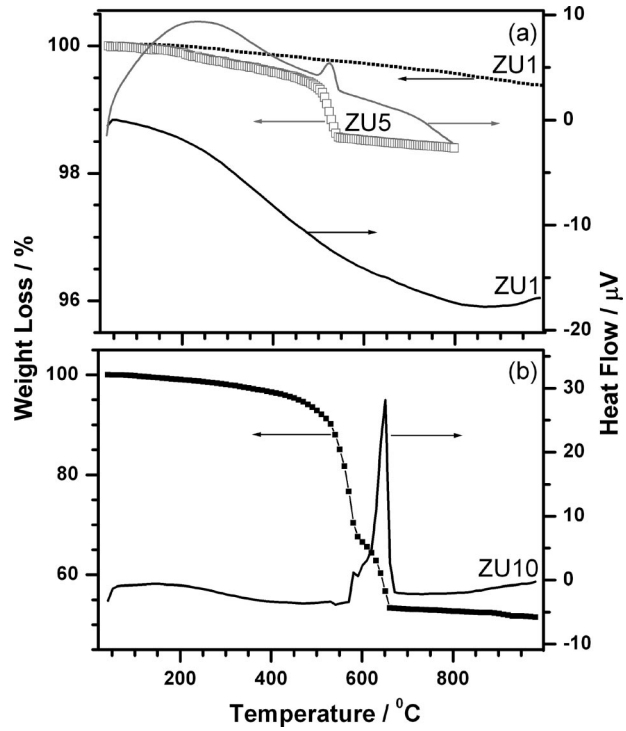


**Figure 3.** Thermogravimetric and differential thermal analysis (TG-DTA) of (a) ZU1 and ZU5 and (b) ZU10, conducted in an air atmosphere at a heating rate of 10 °C/min. In panel (a), the black lines/symbols indicate ZU1, and the gray lines/symbols indicate ZU5. Note the similarity in weight loss pattern for ZU5 and ZU10.

The thermal analysis of ZU1 (Figure 3a), performed in a simulated air atmosphere, exhibits hardly any weight loss (0.4 wt %) up to 800 °C and indicates high thermal stability. No considerable weight loss is observed at <500 °C, because of the loss of any physisorbed $H_2O$ and $NH_3$, or nitrate decomposition, which suggests the high purity of $ZnO_{1-x}N_x$ materials and especially the hydrophobic nature. A broad endotherm observed from 300 °C to 850 °C in DTA suggests some desorption. Indeed, nitrogen desorption is expected above the yellow flame temperature, which is >600 °C. Also note that the lattice parameter of ZU1-950 and ZnO are comparable (see Table 1). Furthermore, the oxidation of $ZnO_{0.85}N_{0.15}$ (ZU1) to ZnO should lead to a marginal weight gain (0.37%). Nonetheless, an overall weight loss (0.4 wt %) observed is attributed to a net oxygen loss throughout the heating in the TG-DTA experiment, rather than the weight gain via the oxidation of $ZnO_{1-x}N_x$ to ZnO at >600 °C. The EDX analyses of ZU1-500 and ZU1 are comparable, indicating that the stoichiometry remains the same for materials annealed up to 500 °C. The aforementioned points and preparation of $ZnO_{1-x}N_x$ via the combustion method suggests that any nitrogen loss might occur at >500 °C. A systematic loss in color of ZU1 from brown (on as-prepared materials) toward white (after calcination at increasing temperature) also corresponds with the nitrogen loss. Further color changes from orange to white, from ZU3 to ZU10, respectively, supports a decrease in the nitrogen content.

A small but sharp change in weight loss (∼1 wt %) was observed at ∼550 °C on ZU5, with a corresponding exothermic change in DTA (Figure 3a). Weight loss observed with a sharp exothermic peak at ∼550 °C

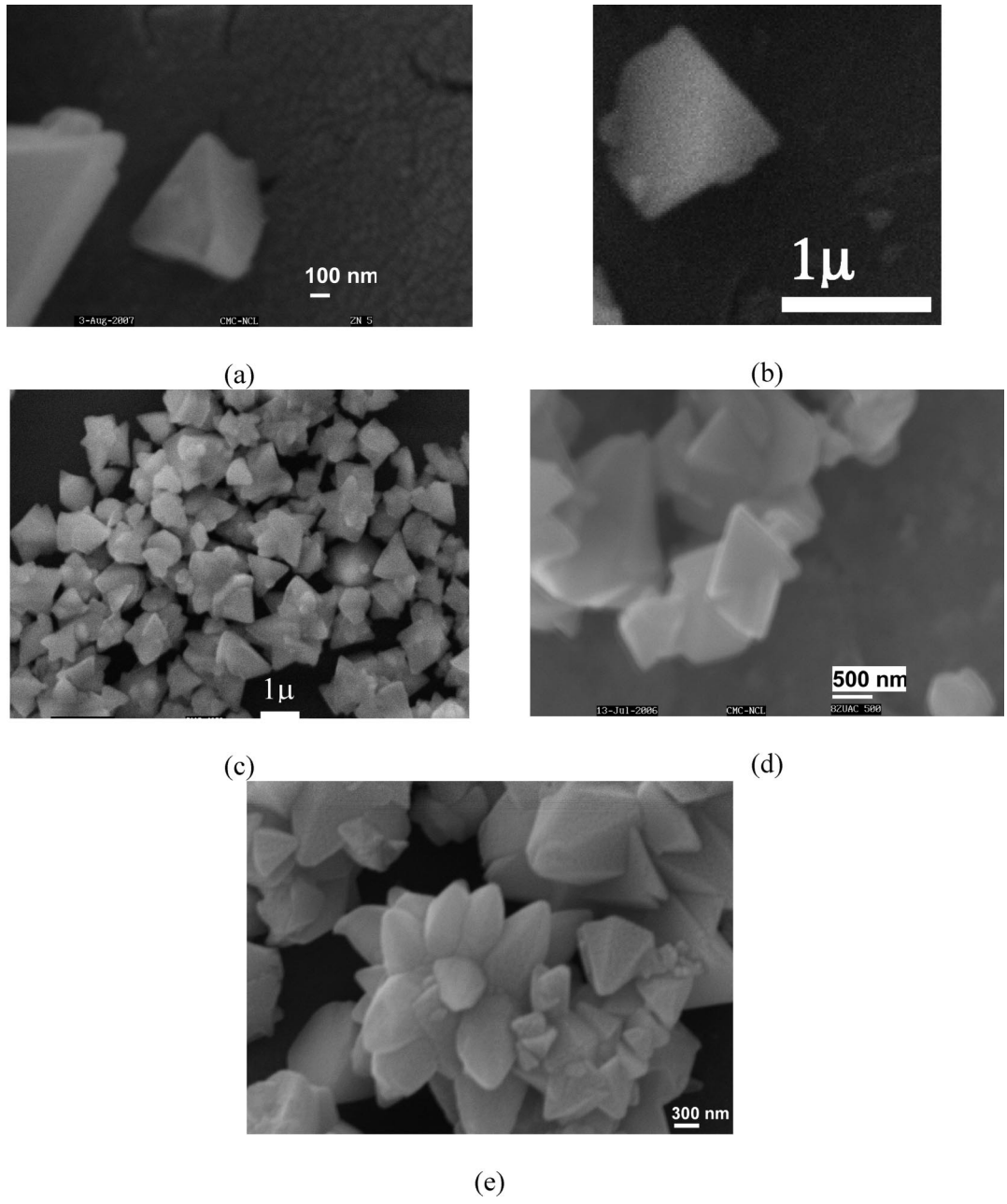


**Figure 4.** Scanning electron microscopy (SEM) images obtained from $ZnO_{1-x}N_x$ materials: (a) ZU0.8, (b and c) ZU1, (d) ZU1-500, and (e) ZU1-650.

suggests a decomposition. To probe this aspect further, ZU10 was also subjected to TG-DTA measurements. When the urea content was increased further in the preparation (for ZU7 and ZU10), the observed weight loss also increases. Very sharp and large weight loss (~40%), accompanied by an exotherm observed in DTA at ~550−660 °C on ZU10 (Figure 3b), is attributed to the decomposition of the carbonate species. Indeed, XPS results support the formation of carbonates between ZU5 and ZU10 (see Figure SI-1 in the Supporting Information). Although a significant intensity of the carbonate decomposition peak was observed for ZU5 (see Figure 3a), a small amount of weight loss at 550 °C and the absence of a carbonate feature in the XRD analysis (see Figure 1) suggests that the carbonate formation is likely limited to surfaces, rather than the bulk. However, a large weight loss in TG and the observation of zinc carbonate diffraction peaks in Figure 1 suggests the bulk nature of zinc carbonate in ZU10.

The morphology of $ZnO_{1-x}N_x$ materials was explored using SEM analysis. The SEM results shown in Figure 4 clearly show that ZU0.8 and ZU1 exhibit triangular and hexagonal-prism-shaped crystals with an edge length of ~400 nm to 1.5 $\mu$m; however, the triangular structure dominates over the prismatic structure. The measured thickness of the triangular particles is ~250 nm, irrespective of the edge length. The uniform contrast that is observed within any triangular or prismatic particle is believed to result from the stress-free and well-grown crystals, which is expected from slow crystallization. It is surprising that such well-grown crystals are observed from the $ZnO_{1-x}N_x$ materials prepared via the SCM method, which is indeed a rapid preparation method. The significant amount of triangular agglomerates that are also observed is attributed to the exposure of smaller

particles to relatively high-temperature zones around flame during combustion preparation. This might be a reason for significantly different atomic composition on individual crystallites measured by EDX. Efforts are also underway to prepare $ZnO_{1-x}N_x$ materials with less fuel, to control agglomeration. After calcination at 500 °C for 6 h, agglomeration increases on ZU1 (Figure 4d); however, sharp edges could still be observed. Calcination to higher temperatures (650 °C) increases the agglomeration and lotus-type agglomerates are observed on ZU1-650. We are yet to understand the mechanism of the triangular-shaped particles under combustion conditions. With a urea:$Zn(NO_3)_2$ ratio of ≥3 in the reaction mixture, no specific particle morphology was observed, and it is attributed to the increasing exothermicity of the combustion reaction. The high urea content in the mixture of reactants makes the combustion better, and it helps to form micropores with a high surface area on ZU7 and ZU10 (see Table 1). Hence, controlled combustion with a stoichiometric urea content (in ZU1 and ZU0.8) produces a well-defined particle morphology. The addition of $NH_4NO_3$, instead of urea, to zinc acetate does produce similar $ZnO_{1-x}N_x$ materials, which suggests the in situ formation of $NH_2/NH_3$ during combustion, and it suggests that the nitrogen source is from urea and not the nitrate nitrogen. *Due to the explosion hazard associated with $NH_4NO_3$, extreme care should be exercised during preparation.* In situ ammonia formation also suggests an overall reduction condition generated under combustion conditions, and it suggests the importance of in situ ammonia formation toward nitrogen introduction into the ZnO lattice than the conventional preparation method, which requires ammonia treatment for several hours at high temperatures.

Figure 5a shows the Raman spectra of ZnO and ZU1 calcined at different temperatures for 6 h. Typical Raman-active modes for ZnO ($E_2$, $A_1$(TO), $A_1$(LO), $E_1$(TO), and $E_1$(LO))[1,10] were also clearly observed for $ZnO_{1-x}N_x$. A sharp and strong peak observed at 437 $cm^{-1}$ on all $ZnO_{1-x}N_x$ and ZnO is due to the $E_2$(Zn−O) mode of the ZnO-wurtzite phase and also indicates the high crystallinity of the material.[1,10] $A_1$(TO) and $E_1$(TO) modes were observed at 380 and 415 $cm^{-1}$, respectively. In addition to the above, three new peaks are observed at 507, 582, and 642 $cm^{-1}$ on $ZnO_{1-x}N_x$. Note that $A_1$(LO) and $E_1$(LO) peaks at ∼580 $cm^{-1}$ are low in intensity for pure ZnO,[10] and the high intensity observed at 582 $cm^{-1}$ is attributed to the $E_2$(Zn−N) mode from $ZnO_{1-x}N_x$. The other two peaks (507 and 642 $cm^{-1}$) are attributed to local vibrational modes of Raman features and these are also identified as Zn−N-related local vibration modes.[10] Comparable intensity of Zn−N (582 $cm^{-1}$) to Zn−O (437 $cm^{-1}$), observed on ZU1, suggests the introduction of a large nitrogen content in ZnO. Also note that the $E_2$(Zn−O) mode at 437 $cm^{-1}$ is much higher in intensity on ZnO than on ZU1, indicating that the Zn−N features are at

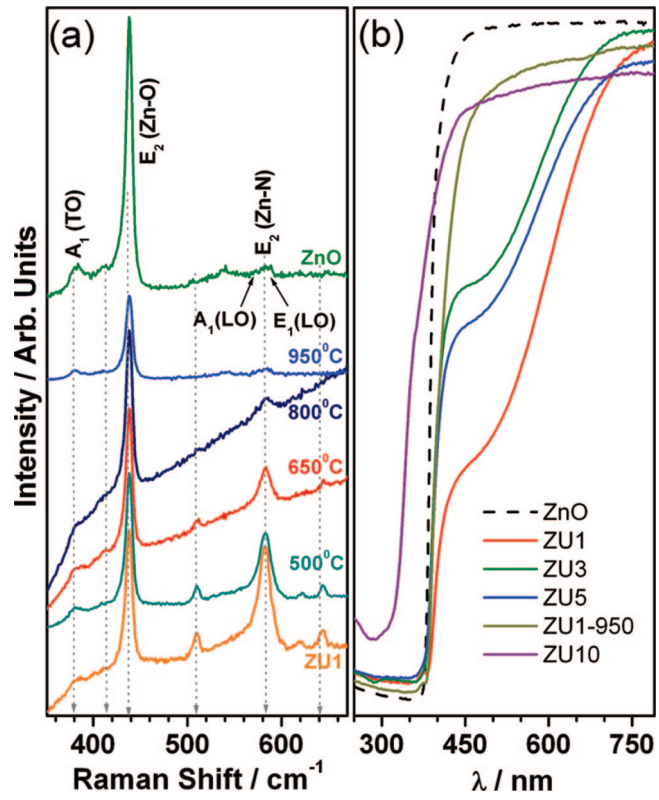


**Figure 5.** (a) Raman spectra of ZnO and ZU1 calcined at different temperatures. (b) Diffuse reflectance UV−vis spectra of the $ZnO_{1-x}N_x$ and ZnO.

the expense of Zn−O features. These changes in intensity underscore the higher covalency of Zn−N than the parent Zn−O bonds. A comparison of the Raman spectra of calcined ZU1 clearly demonstrates a systematic decrease in the intensity of Zn−N vibrational modes. On ZU1-950, all N atoms disappear and show an identical Raman spectrum to that of ZnO. This is direct evidence that supports the Zn−N bonding in $ZnO_{1-x}N_x$.

UV−visible absorption spectra of $ZnO_{1-x}N_x$ materials have been measured, and the results are shown in Figure 5b. ZnO shows an absorption cutoff edge at ∼375 nm.[11] In addition to the above, a new and broad visible absorption band with an absorption onset at ∼600 nm and a band maximum at ∼480 nm is observed on all $ZnO_{1-x}N_x$ materials, except ZU10. The energy difference between the aforementioned two features demonstrates the creation of a midgap (deep level acceptor) state in the band gap. However, despite a high nitrogen content, no hole conductivity was observed and all $ZnO_{1-x}N_x$ materials exhibit insulating characteristics similar to that of ZnO. Indeed, the above observation supports the conclusion that the N 2*p* states are far removed from the top of the O 2*p* valence band. Furthermore, the visible light absorption extends up to 650 nm for $ZnO_{1-x}N_x$, indicating the possibility of utilizing it as a visible light photocatalyst with a suitable co-catalyst. No visible light absorption is observed on ZU1-950, because of the loss of nitrogen, which suggests that the visible light absorption is due to the introduction of nitrogen into the ZnO lattice and the N 2*p*

(10) (a) Yu, J.; Xing, H.; Zhao, Q.; Mao, H.; Shen, Y.; Wang, J.; Lai, Z.; Zhu, Z. *Solid State Commun.* **2006**, *138*, 502. (b) Kaschner, A.; Haboeck, U.; Strassburg, M.; Strassburg, M.; Kaczmarczyk, G.; Hoffmann, A.; Thomsen, C.; Zeuner, A.; Alves, H. R.; Hofman, D. M.; Meyer, B. K. *Appl. Phys. Lett.* **2002**, *80*, 1909. (c) Kerr, L. L.; Li, X.; Canepa, M.; Sommer, A. J. *Thin. Solid. Films.* **2007**, *515*, 5282. (d) Haboeck, U.; Hoffmann, A.; Thomsen, C.; Zeuner, A.; Meyer, B. K. *Phys. Status Solidi B* **2005**, *242*, R21.

(11) Lu, J.; Zhang, Q.; Wang, J.; Saito, F.; Uchida, M. *Powder. Technol.* **2006**, *162*, 33.

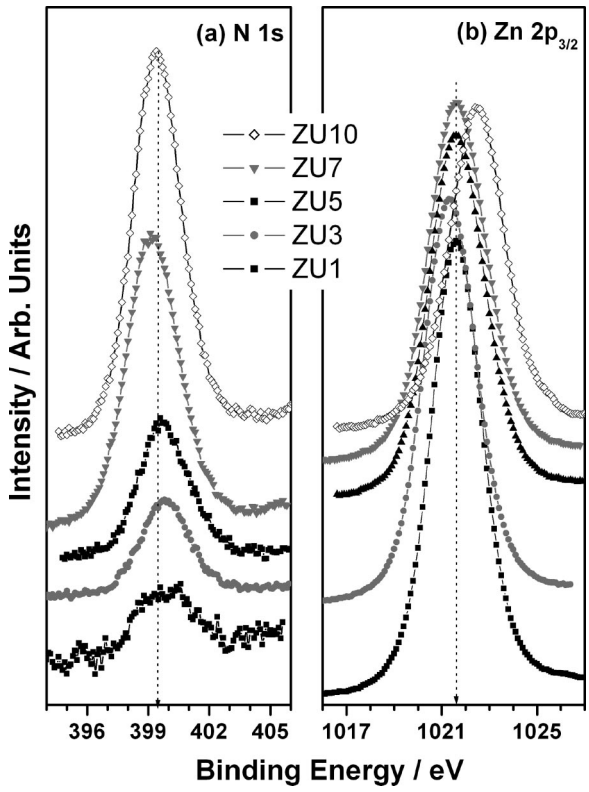


**Figure 6.** (a) N 1*s* core level spectra and (b) Zn $2p_{3/2}$ core level spectra, obtained on $ZnO_{1-x}N_x$.

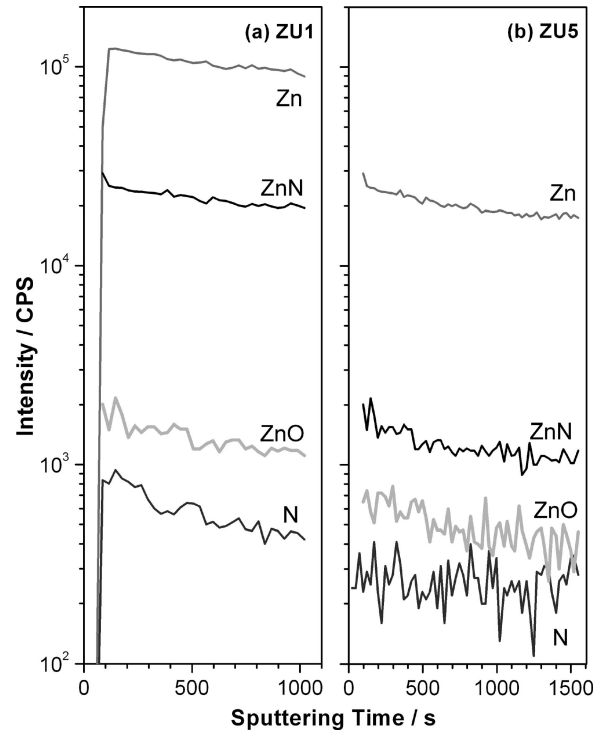


**Figure 7.** SIMS measurements display secondary-ion intensities obtained from (a) ZU1 and (b) ZU5.

derived state. Efforts are underway to decrease the band gap and to induce *p*-type conductivity through co-doping with a suitable donor D ions (where D = Ga or In), along with nitrogen, to make $Zn_{1-z}D_zO_{1-x}N_x$ materials for various applications, including visible light photocatalysis.

XPS spectra of $ZnO_{1-x}N_x$ materials are recorded for N 1*s* and Zn $2p_{3/2}$ core levels and are shown in Figure 6. The N 1*s* core level appears at a binding energy (BE) of 399.4 ± 0.2 eV for all $ZnO_{1-x}N_x$ compositions, which suggests that the electron density on nitrogen remains the same and similar to that of $NH_3$ or amines.[12] The typical nitride ($N^{3-}$) BE is reported to be ~397 eV, and the aforementioned observation suggests that the electron density on nitrogen in $ZnO_{1-x}N_x$ is less than that of nitrides. This might be attributed to a more-covalent character of Zn−N bonds in $ZnO_{1-x}N_x$. However, the surface nitrogen content increases linearly with the amount of urea used in the preparation, which is evident from the aforementioned XPS results. Although ZU10 is colorless, a high surface nitrogen content suggests preferential nitrogen segregation on the surface and is further supported by EDX results. (See Table 1.)

The Zn $2p_{3/2}$ core level appears at BE = 1021.6 eV for all $ZnO_{1-x}N_x$ materials, except ZU10. Indeed, the ZnO BE appears at 1022 eV[12] and suggests that the electron density on Zn in $ZnO_{1-x}N_x$ is slightly higher than that of ZnO. The accommodation of N atoms within the wurtzite structure might possibly lead to a back-donation of electrons, to some extent, from N to Zn; however, this aspect requires further confirmation. The Zn $2p_{3/2}$ level on ZU10, which appears at 1022.5 eV, is attributed to the formation of $ZnCO_3$.

Secondary-ion mass spectroscopy (SIMS) results obtained on $ZnO_{1-x}N_x$ materials, and representative results from ZU1 and ZU5, are shown in Figure 7. Species that exhibit <100 counts/s are not considered, because the noise level is too high. The mass spectrum obtained initially (not shown) displays different species, namely, Zn, N, ZnN, ZnO, and O, with significant to large intensity. Secondary-ion intensities of the first four species are shown in Figure 7, as a function of sputtering time or depth. Qualitatively, the same trend in intensity of all the species is observed on ZU1 and ZU5. No significant decrease in N and ZnN species with sputtering time highlight the bulk nitrogen doping in ZnO, and the uniformity of the substitution throughout the bulk. Nonetheless, ZnN and ZnO species counts are significantly different on ZU1 and ZU5. Considerably large ZnN species on ZU1 underscores that fact that the level of nitrogen doping is higher than ZU5 and corresponds with the values obtained from EDX (see Table 1). Furthermore, higher count rates are observed for ZnN than ZnO, despite ZnO being the host lattice, which is attributed to the different ionization capacity of emitted species, and this is strongly dependent on the local surface characteristics of the materials, known as matrix effect.[13] Generally, an increasing covalent character between the bonding ions makes it difficult to break them, and this might also be an explanation for the higher intensity of Zn−N than

(12) (a) http://srdata.nist.gov/xps/. (b) Vijayaraj, M.; Gopinath, C. S. *J. Catal.* **2006**, *241*, 83. (c) Velu, S.; Suzuki, K.; Gopinath, C. S.; Hattori, T.; Yoshida, H. *Phys. Chem. Chem. Phys.* **2002**, *4*, 1990.

(13) Chakraborty, P. *Ion Beam Analysis of Surfaces and Interfaces in Condensed Matter Systems*; Chakraborty, P., Ed.; Nova Science Publishers: New York, 2002.

Zn−O. An important point to be mentioned here is that no other nitrogen-related species, such as $N_2$, $N_2^{2-}$, NO, $NO_2$, $NO_3$, ZnNO, or $NH_x$, are observed in the mass spectra, which suggests that the status of nitrogen in $ZnO_{1-x}N_x$ material is none of the above. The fact that only one type of nitrogen is observed in all of the aforementioned characterizations underscores the status of nitrogen being unique in $ZnO_{1-x}N_x$ materials, and it is very likely the reason for the replacement of lattice oxygen by nitrogen. Detailed SIMS studies are underway and the same will be reported later.

RT magnetization measured for ZU1 shows apparent dilute ferromagnetic (DFM)[14] behavior, with a typical S-shaped $M(H)$ curve (see Figure SI-2 in the Supporting Information) and is reproduced several times. Nonetheless, the magnetization measured from ZU1 and ZU0.8 (ZU3 and ZU5) corresponds to $2.6 \times 10^{-5}$ ($\sim 2 \times 10^{-5}$) Bohr magneton per ZnO formula unit. The aforementioned DFM characteristics are surprising, because the ZU1-950 (ZnO) sample exhibits linear $M(H)$ behavior at room temperature with no significant magnetic moment (see Figure SI-2 in the Supporting Information), a behavior that is similar to diamagnetism. Thorough analysis of our materials using inductively coupled plasma (ICP) analysis, as well as atomic absorption (AA) analysis, reveals no magnetic impurities (such as Mn, Fe, Co, or Ni) in the $ZnO_{1-x}N_x$, which suggests that the magnetic moment might result because of the nitrogen. Nevertheless, despite all precautions, a trace amount of magnetic impurities that might come from starting chemicals and/or handling the materials at various stages cannot be ruled out.[15] Especially, the combustion condition creates a reductive atmosphere and a trace amount of transition-metal oxides could reduce them to ferromagnetic (FM) metal, and, hence, a DFM behavior is a possibility. Hence, no definitive evidence yet exists and further careful studies are essential.

EPR studies that have been conducted at room temperature on ZU1 and ZU1-950 are shown in Figure 8. This figure shows features that are due to Zn vacancies at $g = 2.00$, but relatively small intensity for oxygen vacancies at $g = 1.96$. No features due to nitric oxide (NO)-type species are observed, which suggests the absence of direct N−O linkages. This is further supported by XPS studies (see Figure 6a), in which no N 1*s* peak was observed at >400 eV. No significant change in intensity is observed for the above features after calcinations at 950 °C; however, a overall decrease in intensity of other features, mostly due to localized defects, is observed. The aforementioned observations also supports the room-temperature ferromagnetic (FM) behavior

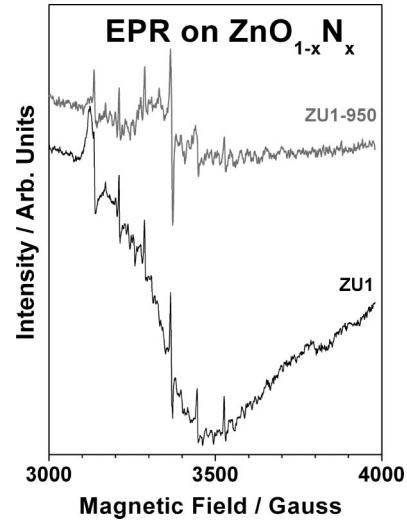


**Figure 8.** Magnetization measured at room temperature for ZU1 and ZU1-950 $ZnO_{1-x}N_x$ materials.

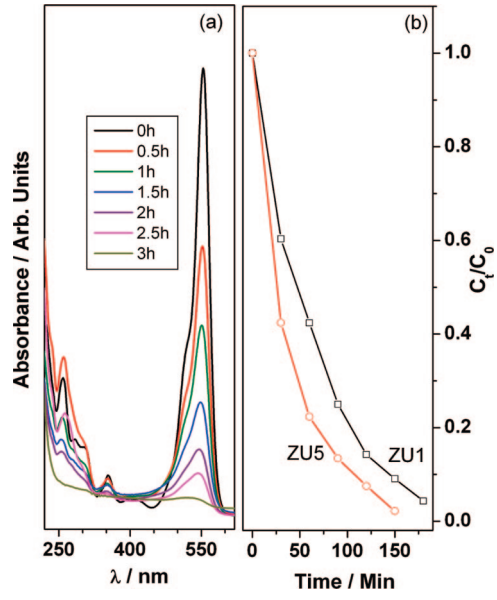


**Figure 9.** (a) UV−visible absorption spectra of rhodamine B decomposition, plotted as a function of UV-light illumination time on ZU1. (b) Photocatalytic decomposition profiles of rhodamine B on ZU1 and ZU5.

(see Figure SI-2 in the Supporting Information) that is observed is due to nitrogen, and it may not be due to oxygen vacancies. A recent report on FM behavior observed on nano-ZnO was attributed to surface O-vacancies and F-centers.[16] However, the particle size observed on $ZnO_{1-x}N_x$ is much bigger and number of defects is likely to be less.

Photocatalytic activity of $ZnO_{1-x}N_x$ was examined through the photodecomposition of rhodamine B solution. One hundred milligrams of $ZnO_{1-x}N_x$ catalyst was suspended in 100 mL of rhodamine B solution and used for photocatalysis studies. The concentration of rhodamine B was determined by monitoring the intensity changes from the absorbance band at 532 nm. Figure 9a shows the changes in the UV−vis absorption spectra of rhodamine B concentration for a reaction period of 3 h of photocatalytic decomposition with

(14) (a) Jayakumar, O. D.; Gopalakrishnan, I. K.; Kulshreshtha, S. K. *Adv. Mater.* **2006**, *18*, 1857. (b) Sharma, P.; Gupta, A.; Rao, K. V.; Owens, F. J.; Sharma, R.; Ahuja, R.; Guillen, J. M. O.; Johansson, B.; Gehring, G. A. *Nat. Mater.* **2003**, *2*, 673. (c) Ueda, K.; Tabata, H.; Kawai, T. *Appl. Phys. Lett.* **2001**, *79*, 988. (d) Rode, K.; Anane, A.; Mattana, R.; Contour, J. P.; Durand, O.; LeBourgeois, R. *J. Appl. Phys.* **2003**, *93*, 7676. (e) Deka, S.; Joy, P. A. *Chem. Mater.* **2005**, *17*, 6507. (f) Deka, S.; Pasricha, R.; Joy, P. A. *Chem. Mater.* **2004**, *16*, 1168. (g) Kittilstved, K. R.; Liu, W. K.; Gamelin, D. R. *Nat. Mater.* **2006**, *5*, 291. (h) Chambers, S. A.; Schwartz, D. A.; Liu, W. K.; Kittilstved, K. R.; Gamelin, D. R. *Appl. Phys. A: Mater. Sci. Process.* **2007**, *88*, 1.

(15) Abraham, D. W.; Frank, M. M.; Guha, S. *Appl. Phys. Lett.* **2005**, *87*, 252502.

(16) Sundaresan, A.; Bhargavi, R.; Rangarajan, N.; Siddesh, U.; Rao, C. N. R. *Phys. Rev. B* **2006**, *74*, 161306.

ZU1. The aforementioned measurements demonstrate the complete decomposition of rhodamine B within 3 h for ZU1 (and ZU5). For a better understanding, the degradation rate of rhodamine B ($\ln(C_t/C_0)$) is plotted against illumination time in Figure 9b for ZU1 and ZU5. The initial 10 ppm concentration of rhodamine B was taken as $C_0$ and $C_t$ is the concentration measured after a specific reaction time. The rate of degradation of rhodamine B shows that it follows approximately pseudo-first-order kinetics: $kt = \ln(C_t/C_0)$, where $k$ is the apparent reaction rate constant (the value of which was determined to be 0.017 and 0.024 $min^{-1}$ for ZU1 and ZU5, respectively). ZU5 shows a relatively higher decomposition rate, and it is attributed to a higher nitrogen content on the surface.

Recently, ZnO has been used for alkylation and acylation reactions,[17] and, here, we demonstrate that $ZnO_{1-x}N_x$ exhibits acylation activity with high selectivity in a simple pot reaction (see Figure SI-3 in the Supporting Information). The acylation of anisole with acetyl chloride was performed at room temperature with $ZnO_{1-x}N_x$ (ZU1 and ZU5). Although anisole conversion is ~50%, the selectivity of 4-methxoy-acetophenone remains high (95%) on both ZU1 and ZU5 and it is worth exploring for other reactions catalyzed by ZnO. Two minor products are observed: mono-orthoacetylated and di-orthoacetylated anisole methxoyacetophenone, with a total selectivity of ~5%. The selective oxidation of cyclohexanol to cyclohexanone and secondary alcohols to corresponding ketones was performed in a fixed-bed reactor in the temperature range of 300−400 °C. Note that product selectivity was observed to be >95% in the previously mentioned two cases. It is likely that the nitrogen present in $ZnO_{1-x}N_x$ might be helpful for high product selectivity. More details on the reaction and analysis will be published elsewhere.

## Conclusions

$ZnO_{1-x}N_x$ materials were prepared using a simple solution combustion method, and it has been characterized by a variety of physicochemical, structural, spectroscopy, microscopy, and magnetic measurements. Except for a minor lattice contraction, no significant change in the ZnO-wurtzite structure was observed, even with 15% nitrogen in $ZnO_{1-x}N_x$. Density measurements suggest the presence of some amount of interstitial Zn when the nitrogen content is high (15%). Charge neutrality of the entire lattice, because of the high nitrogen content in $ZnO_{1-x}N_x$, is maintained by the aforementioned interstitial Zn species and some oxygen vacancies. Nanometer- to micrometer-sized and triangular/prism-shaped particles were observed via SEM. High thermal stability was identified from thermal analysis. Raman, SIMS, and optical studies demonstrate the direct Zn−N bond and the N 2*p* states forms the midgap (deep level acceptor) states, respectively. XPS indicates that the charge density of nitrogen on $ZnO_{1-x}N_x$ is similar to that of $NH_3$. The photocatalytic decomposition of rhodamine B on $ZnO_{1-x}N_x$ with UV light reveals its effectiveness. No significant visible-light photocatalytic activity and the insulating character of $ZnO_{1-x}N_x$ suggest that the N 2*p* states do not change the band gap of $ZnO_{1-x}N_x$, compared to ZnO, because N 2*p* states are in the forbidden region of the bandgap. $ZnO_{1-x}N_x$ materials also exhibit highly selective acylation catalytic activity at room temperature. Visible-light absorption and a large nitrogen content observed, along with the presence of triangular or prismatic shapes, suggests a high potential associated with $ZnO_{1-x}N_x$ toward applications, such as low-threshold semiconductor lasers and photocatalysts such as nitrogen-doped $TiO_2$.[18] The incorporation of a suitable dopant on $ZnO_{1-x}N_x$ or a co-doping of nitrogen with another metal ion[19] might change the properties, especially conduction properties, favorably toward the above applications via band gap engineering. Further detailed studies are underway and will be reported elsewhere.

**Acknowledgment.** We dedicate this work to Prof. Sankaran Subramanian (currently at NCI, NIH, Bethesda). We sincerely thank one of the reviewers, who suggested density measurements to identify the charge compensation mechanism in $ZnO_{1-x}N_x$ materials. C.S.G. thanks Dr. S. Sivaram for encouragement. We thank Dr. D. Srinivas (NCL, Pune), Prof. P. Chakraborty (SINP, Kolkatta), and Dr. K. V. G. K. Murti (AU-KBRC, Chennai) for EPR, SIMS, and Raman spectroscopy measurements, respectively, as well as discussions. Thanks are also due to Mr. R. K. Jha for surface area and thermal analysis and to Mr. A. B. Gaikwad for SEM measurements. M.M. thanks CSIR, New Delhi for a research fellowship.

**Supporting Information Available:** Figures showing XPS analysis results from carbon and oxygen core levels (Figure SI-1), magnetization data (Figure SI-2), and catalytic acylation reaction results of $ZnO_{1-x}N_x$ materials (Figure SI-3). (PDF files.) This material is available free of charge via the Internet at http://pubs.acs.org.

CM803048H

(17) Sarvari, M. H.; Sharghi, H. *J. Org. Chem.* **2006**, *71*, 6652.

(18) Sathish, M.; Viswanathan, B.; Viswanath, R. P.; Gopinath, C. S. *Chem. Mater.* **2005**, *17*, 6349.

(19) Mapa, M.; Saha, B.; Chakraborty, P.; Janet, C. M.; Viswanath, R. P.; Nair, C. M.; Murti, K. V. G. K.; Gopinath, C. S. To be submitted.